VIROLOGY

HIV-1 Gag specifically restricts PI(4,5)P2 and cholesterol mobility in living cells creating a nanodomain platform for virus assembly

C. Favard[1]*, J. Chojnacki[2,3]*, P. Merida[1], N. Yandrapalli[1], J. Mak[4], C. Eggeling[2,5,6†], D. Muriaux[1†]

HIV-1 Gag protein assembles at the plasma membrane of infected cells for viral particle formation. Gag targets lipids, mainly PI(4,5)P2, at the inner leaflet of this membrane. Here, we address the question whether Gag is able to trap specifically PI(4,5)P2 or other lipids during HIV-1 assembly in the host CD4$^+$ T lymphocytes. Lipid dynamics within and away from HIV-1 assembly sites were determined using super-resolution microscopy coupled with scanning fluorescence correlation spectroscopy in living cells. Analysis of HIV-1–infected cells revealed that, upon assembly, HIV-1 is able to specifically trap PI(4,5)P2 and cholesterol, but not phosphatidylethanolamine or sphingomyelin. Furthermore, our data showed that Gag is the main driving force to restrict the mobility of PI(4,5)P2 and cholesterol at the cell plasma membrane. This is the first direct evidence highlighting that HIV-1 creates its own specific lipid environment by selectively recruiting PI(4,5)P2 and cholesterol as a membrane nanoplatform for virus assembly.

INTRODUCTION

During HIV-1 replication cycle, the assembly and release of newly made viral particles occurs at the plasma membrane of the infected cells (Fig. 1A). Budded HIV-1 particles display an unusual lipid membrane composition that differs notably from that of the plasma membrane of the host cell. It is enriched in sphingomyelins (SMs), glycosphingolipids, cholesterol (Chol), and phosphoinositides, such as phosphatidylinositol 4,5-bisphosphate lipid [PI(4,5)P2] (*1*, *2*), and characterized by highly ordered, i.e., densely packed, lipid organization (*1*, *3*). This raises the question on how virus components interact with lipids in the plasma membrane of the host cells to gather such specific lipid environment during assembly. For instance, PI(4,5)P2 is recognized by the N-terminal region of HIV-1 Gag proteins that targets Gag to the plasma membrane (*4*–*6*). Then, studies of HIV-1 lipid interactions were mainly based on in vitro model systems (*7*–*11*), tagged phospholipid-interacting protein domains (*12*), or virus lipidomics (*1*, *2*, *7*). However, direct observations of the relevant molecular interactions in the living cells have long been challenged by the limited spatial resolution of conventional optical microscopy. Fortunately, recent advances in super-resolution microscopy techniques have enabled for the characterization of molecular mobility at the nanoscale, i.e., on the scale of individual (<140 nm) HIV-1 particles. For example, experiments using a combination of super-resolution [stimulated emission depletion (STED) microscopy and fluorescence correlation spectroscopy (STED-FCS) (*13*) or scanning STED-FCS (sSTED-FCS) (*14*, *15*)] revealed a low mobility of molecules on the HIV-1 surface (*3*) due to the high degree of lipid packing in the virus membrane (*15*, *16*).

The retroviral protein Gag is thought to be a key player in altering the HIV-1 lipid environment, as it is not only the main structural determinant of the particle assembly but also mediates the interactions between assembling virus particle and plasma membrane lipids. HIV-1 Gag is composed of four domains (MA, CA, NC, and p6) and two spacer peptides (sp1 and sp2). The MA domain of Gag is myristoylated on its N terminus and contains a highly basic region (named HBR), both responsible for Gag anchoring and targeting to the cell plasma membrane (*4*–*6*, *17*). The CA domain is involved in the Gag-Gag interaction for multimerization. The NC domain is required for genomic RNA encapsidation and also for Gag-Gag multimerization through RNA (*18*). The p6, and part of the NC domain, recruits host cell factors for particle budding (*19*). The space peptide sp1 is also required for proper particle assembly and budding (*20*). The binding of Gag to the plasma membrane is primarily resulting from a bipartite signal within MA [reviewed in (*17*)]. It is understood that MA is thought to interact with the acidic lipids of the plasma membrane inner leaflet (*4*), although recent studies suggest that the NC domain of Gag could also play a role (*21*). Substitutions of the MA basic residues have been shown to affect the targeting and membrane binding of HIV-1 Gag both in liposomes (*22*) and in cells (*5*). Furthermore, a lipidomic study has suggested that Gag interacts with acidic phospholipids in cells, since virions produced by HIV-1–infected cells were enriched in PI(4,5)P2 via an MA-dependent manner (*2*), and this interpretation is supported by a recent report using a tunable PI(4,5)P2 level to track Gag anchoring onto the cell membrane via imaging analysis (*23*).

The unusual lipid contents in HIV-1 show that HIV-1 particles require a specific lipid membrane environment for HIV-1 assembly. A key question in HIV-1 assembly is whether Gag is targeted toward preexisting lipid domains at the plasma membrane or whether Gag actively creates its unique lipid compositions for virus formation. Historically, Gag has been shown to associate with the detergent-resistant membrane fractions (*24*, *25*), which are enriched in SM and Chol, and raft properties of the virion-cholesterol impact on virus function (*26*, *27*). Saad *et al.* (*28*) have used truncated acyl chains PI(4,5)P2 to show that the unsaturated *sn-2* acyl chain of the PI(4,5)P2 is trapped in an hydrophobic pocket, while the myristate is embedded into

[1]Montpellier Infectious Disease Research Institute, IRIM, CNRS–Université Montpellier, 1919, route de Mende, 34293 Montpellier Cedex, France. [2]MRC Human Immunology Unit, Weatherall Institute of Molecular Medicine, University of Oxford, Oxford OX3 9DS, UK. [3]IrsiCaixa AIDS Research Institute, University Hospital Germans Trias i Pujol, Ctra. de Canyet s/n, Badalona, 08916 Barcelona, Spain. [4]Institute for Glycomics, Griffith University Gold Coast, Southport, QLD, Australia. [5]Institute of Applied Optics and Biophysics, Friedrich-Schiller-University Jena, Max-Wien Platz 4, 07743 Jena, Germany. [6]Leibniz Institute of Photonic Technology e.V., Albert-Einstein-Straße 9, 07745 Jena, Germany.
*These authors contributed equally to this work.
†Corresponding author. Email: delphine.muriaux@irim.cnrs.fr (D.M.); christian.eggeling@rdm.ox.ac.uk (C.E.)

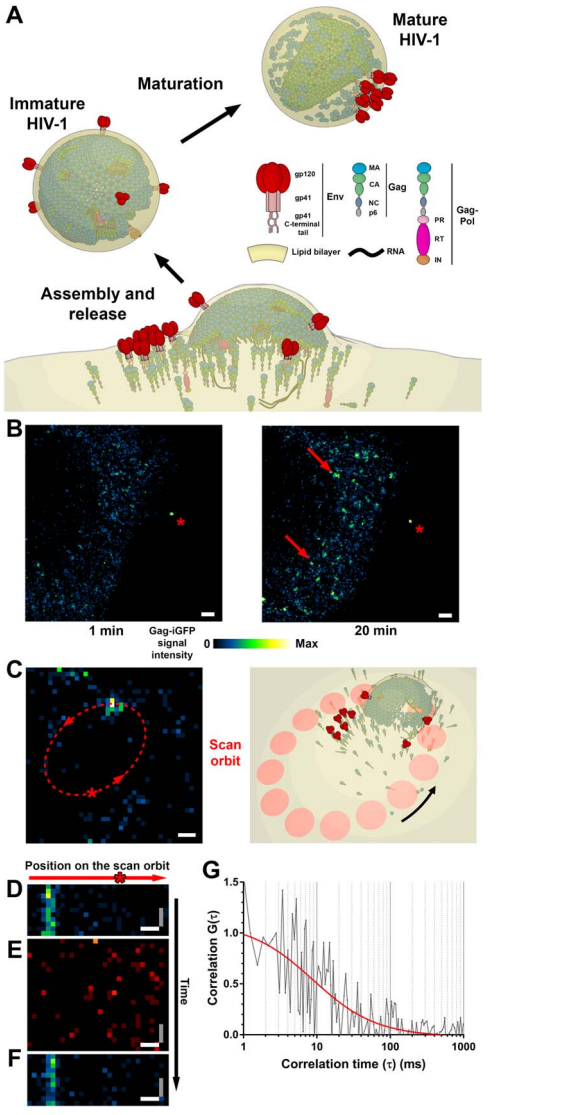

Fig. 1. sSTED-FCS measurement of lipid diffusion inside and outside HIV-1 assembly sites. (**A**) Schematic illustration of Gag and Env distribution during HIV-1 assembly, release, and maturation. (**B**) Representative confocal time lapse images of Jurkat T cells infected with NL4.3 Gag-iGFP HIV-1. On day 3 after infection, cells were adhered to poly-L-lysine–coated coverslips and monitored for the appearance of HIV-1 assembly sites prior to sSTED-FCS measurements. Images represent Gag-iGFP signal (blue-green-yellow) at the cell-coverslip interface at 1 (left) and 20 min (right) after adherence. Arrows indicate the appearance of the individual diffraction-limited HIV-1 assembly sites, which were subsequently analyzed by sSTED-FCS. A cell-free HIV-1 particle is indicated by an asterisk. Scale bar, 1 μm. (**C**) Left: Live confocal imaging was used to localize HIV-1 virus assembly sites using Gag.iGFP signal (blue-green-yellow) as a guide and to align them with the position of the circular scan orbit (red dashed line). Right: Schematic illustration of sSTED-FCS orbit over the HIV-1 assembly site. Arrows indicate the direction of the scan. Scale bar, 200 nm. (**D** to **F**) Representative confocal-mode signal intensity carpets for Gag. iGFP signal (blue-green-yellow) before (D) and after (F) acquisition of STED-mode intensity carpet for lipids (here, PE-ATTO647N) (E) inside and outside HIV-1 assembly sites. Image *x* and *y* axes correspond to the position on the scan line and signal intensity at each time point, respectively. Scale bars, 200 nm (*x* axis; white); 1.24 ms (*y* axis; gray). (**G**) Representative normalized autocorrelation curve of PE-ATTO647N diffusion (gray line) obtained from a single position [marked by the red asterisk in (C) and (D) to (F)] on the circular scan line within the correlation carpet. Autocorrelation curve (red) was fitted using a generic 2D diffusion model.

the lipid membrane, leaving the complex MA:PI(4,5)P2 to partition to more liquid-ordered membrane environments. Using phase-separated giant unilamellar vesicles (GUVs), Keller *et al.* (*9*) have shown that multimerizable MA domains are partitioning into more liquid-disordered membrane environments. In addition, using coarse-grained molecular dynamics, researchers have highlighted that HIV-1 MA interacts only with PI(4,5)P2 sugar head and that PI(4,5)P2 is concentrated within the immediate vicinity of MA (*29*). Recent nuclear magnetic resonance studies on HIV-1 MA in interactions with lipidic membranes confirmed these results and disproved the model that the unsaturated *sn-2* acyl chain of PI(4,5)P2 is trapped in a hydrophobic pocket of MA (*30*). Last, our recent lipidic membrane–based study demonstrated that recombinant HIV-1 Gag was able to segregate PI(4,5)P2 and cholesterol-BOron-DIPYrromethene (BODIPY) fluorescent analogs but excluded the BODIPY-SM analog upon Gag multimerization and that Gag preferred to partition into the PI(4,5)P2 analog–enriched liquid-disordered lipid membrane environments on GUVs rather than liquid-ordered lipid membrane environments (*10*). Together, these results suggest that HIV-1 Gag may generate its own PI(4,5)P2-enriched membrane environment at the cell plasma membrane rather than assembling on preexisting areas or domains with distinct lipid membrane environments. This is consistent with a study using a biological tool to tune PI(4,5)P2 level at the cell plasma membrane, and it was recently reported that PI(4,5)P2 not only targets Gag to the cell membrane but also is necessary for assembly site formation (*23*).

To study this dynamic equilibrium of Gag-lipid interaction in living host CD4$^+$ T cells, here, we use the super-resolution sSTED-FCS approach to analyze the mobility of fluorescent lipid analogs inside and outside HIV-1 assembly sites on fluorescent Gag-labeled CD4 T cells infected by HIV-1 or expressing Gag only. We find that infectious HIV-1 is able to immobilize PI(4,5)P2, and Chol, but not phosphatidylethanolamine (PE) and SM analogs in these host cells and that only Gag is required to restrict the movement of these lipid molecules at the assembly sites. Our results highlight that HIV-1 Gag selectively traps PI(4,5)P2 and cholesterol in host CD4 T cells to create its own specialized lipid membrane environment for virus assembly.

RESULTS

PI(4,5)P2 and cholesterol, but not SM analogs, are trapped during HIV-1 assembly in infected CD4$^+$ T cells

Assembly of fully infectious HIV-1 particles requires a concomitant assembly of viral Env and Gag/GagPol at the assembly site, i.e., at the cellular plasma membrane, involving specific lipid environments that can be either preexisting or generated by the viral proteins. To distinguish these possibilities, we infected Jurkat CD4$^+$ T lymphocytes with infectious NL4.3 HIV-1 viruses. These viruses expressed green fluorescent protein (GFP), which was inserted between the MA and CA domains of Gag (Gag-iGFP) (*31*). The concomitant fluorescence allowed for tracking the movement of fluorescently tagged lipids at HIV-1 assembly sites (Fig. 1A).

Seventy-two hours after infection, we tested whether infected cells are able to support HIV-1 assembly. Time lapse imaging at 37°C of cells adhered to poly-L-lysine–coated coverslips highlighted that infected cells produced newly appearing virus assembly sites within 20 min after adherence (Fig. 1B and movie S1) This is consistent with previous HIV-1 assembly studies of HIV-1 particles (*32*) and HIV-1 Gag virus-like particle (VLP) production in CD4$^+$ T cells (*33*).

To visualize lipid mobility within or outside virus assembly sites, we labeled the $CD4^+$ T cells with fluorescent lipid analogs prior to adhering cells to poly-L-lysine–coated coverslips. The selected analogs correspond to lipids known to be enriched in HIV-1 membranes such as Chol and SM, to have a major role in Gag membrane interaction such as PI(4,5)P2, or to be selectively excluded in HIV-1 membranes such as PE. Figure S1 shows the structures of the lipid analogs used. These analogs have been used multiple times before, and in their cases, the dye label has been shown to have minimal influence on the lipids' membrane interaction dynamics (*34*–*37*). However, the relatively large dye labels on the lipid analogs may prevent them from entering highly ordered membrane environments [as highlighted before in (*38*)]. These highly ordered membrane environments may also be created at the Gag assembly sites. However, as reported below, we see distinct differences between different lipid types using the same label, indicating that it is not the label but rather the lipid that is dominating the organizational and interaction properties of the analog. In addition, using classical spot FCS, we first confirmed that the mobility of these lipid analogs in $CD4^+$ T cells was comparable between different dye labels, specifically to the mobility observed with corresponding BODIPY-labeled lipids (fig. S2).

To acquire lipid analog mobility data via sSTED-FCS, we aligned fluorescent HIV-1 assembly sites with the laser scanning orbit of our microscope using a Gag-iGFP fluorescence signal as a guide (Fig. 1C). Figure S2 highlights (for the case of the SM analog) that beam scanning per se did not change the results obtained [as highlighted before in (*14*)]. In our current sSTED-FCS measurements, we first took larger confocal microscope images identifying spots of GFP fluorescence as relevant Gag clustering sites, and for subsequent analysis, we only selected newly appearing (after cell adherence to the coverslip) small and immobile (during the acquisition) Gag clusters at the T cell surface with low-fluorescence Gag signal intensity. Previous studies have shown that these sites represent virus assembly that is still in progress (*32*) and thus minimize the risk of performing fluorescent lipid analog mobility analysis on the site of already budded virus particles (see also fig. S3). After this identification step, the microscope was switched from imaging (*x* and *y* axes) to continuous orbital line scanning (*x* and *t* axes, intensity carpet acquisition) mode. Consequently, we recorded temporal fluorescence intensity fluctuations at each position (or pixel) along the scanned orbit. An orbit always included Gag-clustering sites and thus HIV-1 assembly sites (GFP fluorescence) and areas without Gag (no GFP fluorescence) (Fig. 1). We first acquired a short intensity carpet for Gag fluorescence in a confocal mode to ensure that (i) the scanning orbit was correctly overlapped with the position of the virus assembly site and (ii) the Gag assembly site was sufficiently immobile (no shift detected along the *x* axis of the intensity carpet for Gag fluorescent signal) to enable lipid mobility measurements (Fig. 1D). Afterward, we acquired an intensity carpet for the red emission signal of the fluorescent lipid analogs with a reduced observation spot size (diameter, ~100 nm; STED microscopy mode) (Fig. 1E). The reduced observation spot size ensured that we are indeed mainly covering lipid data at the assembly site only and not averaging over a larger nonrelevant area. Last, we again recorded a fluorescence intensity carpet of Gag fluorescence in the confocal mode to further ensure that the virus assembly site shows no detectable drift during the whole acquisition process (Fig. 1F). The acquisition parameters for the recording of the fluorescent lipid analog data were chosen for reducing bias and for generating accurate data: (i) The spot size of 100 nm in diameter ensured sufficient spatial resolution (fig. S4) for distinguishing trapped from nontrapped lipids in and out of individual virus assembly sites and yet had still high enough signal-to-noise ratios for reasonable and reproducible FCS data (see error bars further on). (ii) Orbital beam scanning with 3.23 kHz realized a low enough dwelling at each scanned point to minimize (excitation and STED) laser exposure and thus phototoxic effects (*39*), as well as a high enough temporal resolution of the decaying FCS data (*40*). (iii) The number of total points (30) per orbital scan facilitated the collection of sufficiently enough data points for an accurate identification of the virus assembly sites (*14*). FCS data were generated for each point along the orbital scan and fitted with a generic two-dimensional (2D) diffusion model to obtain the average transit times through the observation spot and the apparent diffusion coefficient (D_a) of the lipid analogs at each location (Fig. 1G).

Figure 2 shows the change in lipid analog lateral mobility observed in infected Jurkat T cells within (red boxes) and outside (green boxes) the HIV-1 assembly sites. The lateral mobility of the lipid analogs as measured in uninfected control cells is presented in blue. As previously observed for ATTO647N-PI(4,5)P2 and TopFluor PI(4,5)P2 in supported lipid bilayers (SLBs) [fig. S5 and (*10*)], the median diffusion coefficient of ATTO647N-PI(4,5)P2 (Fig. 2A) within the assembly sites was strongly reduced [D_a = 0.02 $\mu m^2/s$, interquartile range (IQR) = 0.09 $\mu m^2/s$] compared to the one observed outside the assembly sites (D_a = 0.17 $\mu m^2/s$, IQR = 0.31 $\mu m^2/s$) or in HIV-1–negative cells (D_a = 0.20 $\mu m^2/s$, IQR = 0.30 $\mu m^2/s$). Therefore, in infected Jurkat T cells, the general mobility of ATTO647N-PI(4,5)P2 was decreased 8- to 10-fold within the assembly sites compared to elsewhere or in HIV-1–negative cells. We further tested the Gag-specific mobility of Chol. Chol has been shown to play a major role in the assembly process of HIV-1 virus (*24*). When monitoring the diffusion coefficient of Chol-PEG-KK114 (Fig. 2B), we observed a similar decrease of Chol analog mobility (D_a = 0.10 $\mu m^2/s$, IQR = 0.20 $\mu m^2/s$) within the assembly sites compared to elsewhere (D_a = 0.25 $\mu m^2/s$, IQR = 0.32 $\mu m^2/s$) and in HIV-1–negative cells (D_a = 0.29 $\mu m^2/s$, IQR = 0.32 $\mu m^2/s$). In contrast, the ATTO647N-SM analog did not exhibit any significant change in mobility in the presence or absence of HIV-1 or within and outside the assembly sites (D_a = 0.15 $\mu m^2/s$, IQR = 0.12 $\mu m^2/s$ and D_a = 0.17 $\mu m^2/s$, IQR = 0.16 $\mu m^2/s$ within and outside the assembly sites, respectively, and D_a = 0.15 $\mu m^2/s$, IQR = 0.15 $\mu m^2/s$ in uninfected cells; Fig. 2C). Similarly, we observed no significant change in the mobility of the ATTO647N–1,2-dipalmitoyl-*sn*-glycero-3-phosphoethanolamine (ATTO647N-DPPE) lipid analog within (D_a = 0.32 $\mu m^2/s$, IQR = 0.31 $\mu m^2/s$) versus outside (D_a = 0.31 $\mu m^2/s$, IQR = 0.24 $\mu m^2/s$) the assembly sites or versus uninfected cells (D_a = 0.31 $\mu m^2/s$, IQR = 0.18 $\mu m^2/s$) (Fig. 2D).

We noticed that the values of the apparent diffusion coefficients as determined from the sSTED-FCS (operating with a ~100-nm large observation spot) were generally smaller (D_a = 0.1 to 0.4 $\mu m^2/s$) compared to data taken with confocal FCS (operating with a ~250-nm large observation spot, D_a = 0.7 to 1 $\mu m^2/s$; fig. S2). We have compared values of D_a for different observation sizes in STED-FCS multiple times before to point out molecular diffusion modes of lipid analogs in other cells and membranes (*34*). In the case of hindered diffusion such as transient trapping, we congruently explored a three- to six-times reduction of values of D_a for observation spots with diameters <100 nm compared to those determined for conventional confocal spots (~250 nm). Such transient trapping was also determined for most of the lipid analogs used here (*34*). Consequently, values of D_a determined for <100-nm observation spot sizes are expected to be reduced compared to confocal recordings. However,

the absolute values of D_a were of less relevance since we were interested in highlighting changes in mobility between inside and outside Gag assembly sites.

Expression of HIV-1 Gag alone is sufficient to immobilize PI(4,5)P2 and cholesterol analogs during formation of VLPs

HIV-1 Gag alone is able to self-assemble at the plasma membrane of the Jurkat T cells, leading to the generation of immature VLP. Kerviel *et al.* (*41*) proposed that the self-association of Gag is sufficient to generate a specific lipid environment. Therefore, by transfecting the HIV-1 Gag.eGFP-only expression vector into Jurkat T cells (for more details, see fig. S6) and measuring changes in the mobility of lipids at Gag self-association sites, we tested whether the selective lipid analog clustering that we have observed in HIV-1–infected cells (see above) was also present in Gag-only assembly sites.

As with the infected Jurkat T cells, we first tested for the evidence of appearance of VLP assembly sites at the surface of HIV-1 Gag-expressing Jurkat cells (Fig. 3A), followed by the determination of lipid analog diffusion coefficients both within and outside those sites.

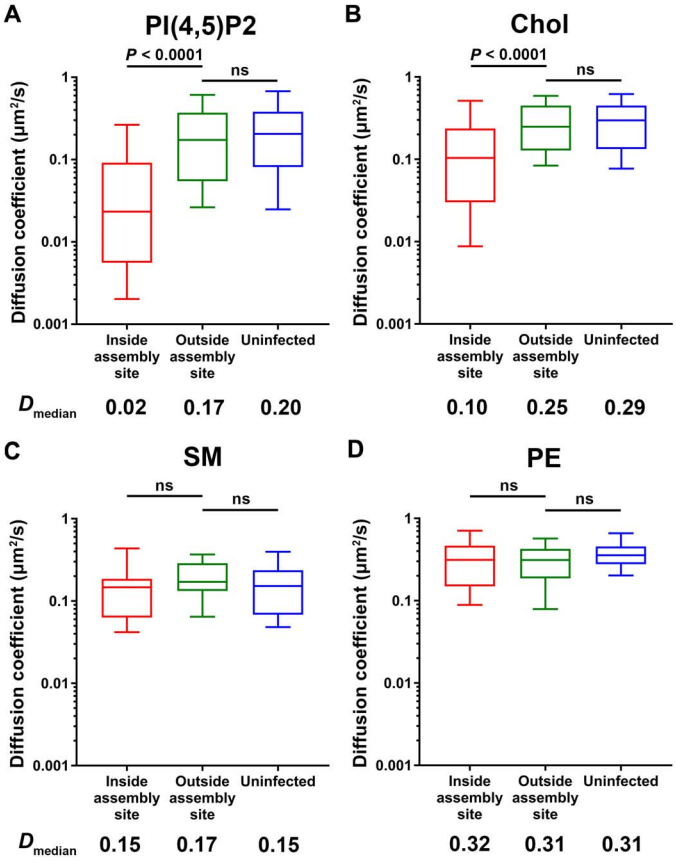

Fig. 2. Lipid mobility changes in NL4.3 Gag-iGFP HIV-1–infected Jurkat T cells. Median lipid diffusion coefficients (D_a) as determined by sSTED-FCS measurements of 20 sites each from two independent virus preparations and infections. Box-and-whisker plots (horizontal line, median; box, 25 to 75% percentiles or IQR; whiskers, 10 to 90% measurements) showing D_a values inside assembly sites (red), outside assembly sites (green), and in noninfected control cells (blue). Data were collected for (**A**) ATTO647N-PI(4,5)P2, (**B**) cholesterol (Chol-PEG-KK114), (**C**) SM (ATTO647N-SM), and (**D**) PE (ATTO647N-DPPE) analogs. Statistical significance was assessed by Wilcoxon rank sum test. ns, not significant.

We determined lipid diffusion at arbitrary sites in nontransfected (non-Gag–expressing) cells as control. Figure 3 (B to E) depicts the different values of diffusion coefficients determined within (red boxes) and outside the assembly sites of HIV-1 Gag VLP (green boxes) and in the nontransfected control cells (blue box). As observed in infected cells, the lateral mobility of ATTO647N-PI(4,5)P2 was significantly reduced inside (D_a = 0.11 μm²/s, IQR = 0.21 μm²/s) compared to outside assembly sites or to nontransfected cells (D_a = 0.24 μm²/s, IQR = 0.31 μm²/s and D_a = 0.20 μm²/s, IQR = 0.30 μm²/s, respectively) (Fig. 3B). However, the reduction in mobility between inside and outside the assembly sites is only 2.2-fold (0.24/0.11) for T cells only expressing HIV-1 Gag VLP in comparison with 8.5-fold (0.17/0.02) for HIV-1–infected T cells. Nevertheless, experiments on model membranes support the direct role of Gag in this process of PI(4,5)P2 trapping. Upon addition of Gag to SLBs with 0.2% of fluorescent PI(4,5)P2 analog, we observed the formation of ATTO647N-PI(4,5)P2 clusters at the Gag binding sites with a concomitant sevenfold decrease in PI(4,5)P2 analog mobility at these sites compared to elsewhere on the SLBs or on SLBs in the absence of Gag (fig. S5). Also in line with our data on infected T cells, we also observed a twofold reduction in the lateral mobility for Chol-PEG-KK114 within the Gag assembly sites (D_a = 0.16 μm²/s, IQR = 0.26 μm²/s) of HIV-1 Gag VLP only expressing T cells, compared to either outside the assembly site (D_a = 0.30 μm²/s, IQR = 0.40 μm²/s) or in nontransfected control cells (D_a = 0.29 μm²/s, IQR = 0.52 μm²/s; Fig. 3C). In contrast, ATTO647N-SM and ATTO647N-DPPE (Fig. 3, D and E, respectively) again exhibited no significant changes in their lateral mobility between HIV-1 Gag self-assembly sites when compared to outside the sites or in nontransfected cells (ATTO647N-SM: inside, D_a = 0.16 μm²/s, IQR = 0.33 μm²/s; outside, D_a = 0.14 μm²/s, IQR = 0.34 μm²/s; nontransfected, D_a = 0.14 μm²/s, IQR = 0.30 μm²/s; ATTO647N-DPPE: inside, D_a = 0.46 μm²/s, IQR = 0.38 μm²/s; outside, D_a = 0.24 μm²/s, IQR = 0.34 μm²/s; nontransfected, D_a = 0.50 μm²/s, IQR = 0.47 μm²/s).

HIV-1 Gag is the primary determinant of lipid trapping efficiency at HIV-1 assembly sites in CD4⁺ T cells

The decrease in the lateral mobility of ATTO647N-PI(4,5)P2 and Chol-PEG-KK114 at Gag assembly sites suggests trapping of these lipid analogs during virus particle formation. To further quantify this restricted diffusion, we used a confinement index based on normalized relative cumulative frequency histograms of the values of the diffusion coefficient D_a (for D_a = 0.001 to 1 μm²/s, normalized to 100 for D_a = 1 μm²/s). Representative cumulative frequency histograms for diffusion within and outside the assembly sites are shown in figs. S7 and S8, respectively, highlighting a huge difference for PI(4,5)P2 and Chol (but not for SM and PE) analogs. To further specify this difference, we classified three diffusion regimes, "fast," "intermediate," and "slow" mobility, for respective values of $D_a < 0.01$, $0.01 \leq D_a < 0.1$, and $D_a \geq 0.1$ μm²/s, we calculated the sum of cumulative frequencies within each regime, and we plotted the confinement index for each regime as the ratio of the latter values for lipid diffusion within and outside the assembly sites or within the assembly sites and noninfected (or nontransfected) cells. For an increased confinement of lipids inside the assembly sites, we would expect a larger relative fraction of low values of D_a, i.e., an increased fraction and thus confinement indices >1 within the intermediate and especially the slow mobility regimes (and consequently a reduced fraction and thus a confinement index <1 within the fast regime). In contrast, similar cumulative frequency histograms and thus confinement

indices ≈1 for all regimes indicate no change in mobility and thus no confinement within the assembly sites. As expected, the various values of confinement indices confirm our previous conclusion, i.e., that ATTO647N-SM and ATTO647N-DPPE did not exhibit any confinement within assembly sites, while ATTO647N-PI(4,5)P2 and Chol-PEG-KK114 revealed a drastic reduction of lateral mobility and thus confinement at the assembly sites.

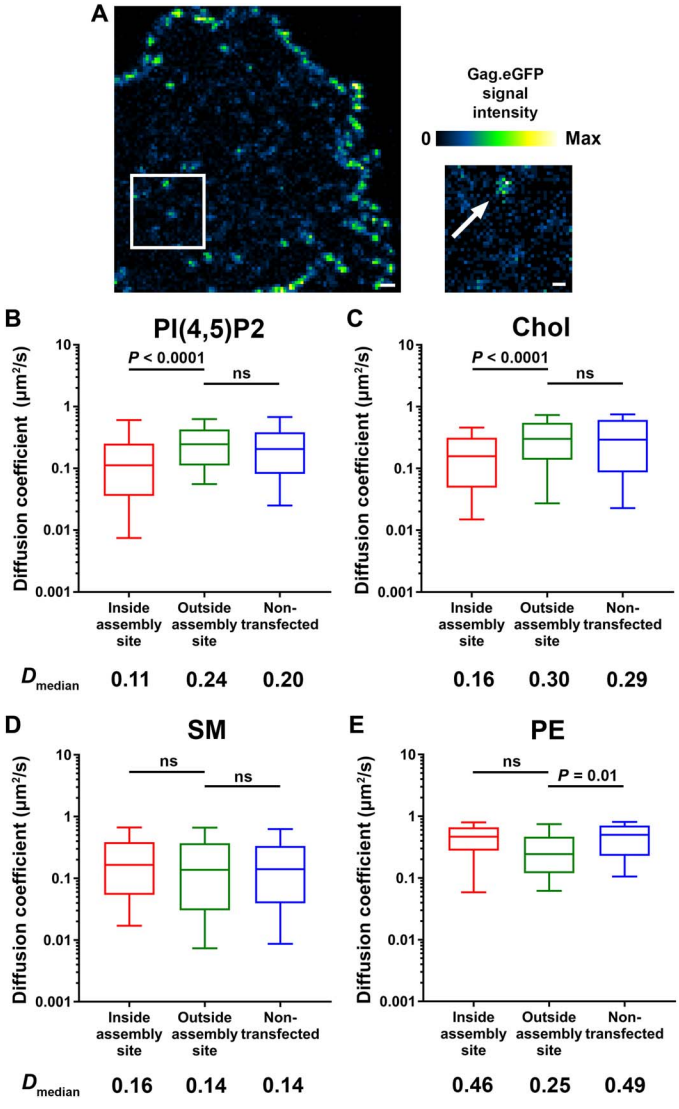

Fig. 3. Lipid mobility changes in HIV-1 Gag.iGFP transfected Jurkat T cells. (**A**) Representative live confocal image of Jurkat T cells expressing HIV-1 Gag.iGFP. Image represents Gag.iGFP signal (blue-green-yellow) at the cell-coverslip interface at 24 hours after transfection. Scale bar, 1 μm. Zoomed-in confocal image depicts an individual HIV-1 assembly site indicated by an arrow. Scale bar, 200 nm. (**B** to **E**) Median values of the lipid diffusion coefficients (D_a) were determined for (A) ATTO647N-PI(4,5)P2, (B) cholesterol (Chol-PEG-KK114), (C) SM (ATTO647N-SM), and (D) PE (ATTO647N-DPPE) analogs by sSTED-FCS on 20 sites each from two independent Gag.iGFP transfections. Box-and-whisker plots (horizontal line, median; box, 25 to 75% percentiles or IQR; whiskers 10 to 90% measurements) showing D_a values inside assembly sites (red), outside assembly sites (green) and in untransfected control cells (blue). Statistical significance was assessed by Wilcoxon rank sum test.

When we compared the confinement index values obtained for the different lipids in HIV-1 Gag-transfected cells (Fig. 4, gray bars) against those in HIV-1–infected cells (Fig. 4, black bars), we observed similarities between these two conditions. Specifically, both PI(4,5)P2 and Chol analogs have values of high confinement indices >1 in the intermediate and slow regimes for both HIV-1–infected and Gag-only–expressing T cells, while confinement index values ≈1 are conserved for both SM and PE analogs. This highlights that the HIV-1 Gag protein on its own seems to be sufficient to facilitate the confinement or trapping of cholesterol and PI(4,5)P2 analogs in HIV-1 assembly sites, and no other molecular factor only present in infected cells (and not in the Gag-only case) is required.

DISCUSSION

How enveloped viruses acquire their lipid membrane shell is of great importance for their biogenesis and their capacity to infect cells. In the case of HIV-1, recently, it has been shown that the envelope lipid composition was a determinant of low molecular mobility of the Env protein (*3*, *16*). Several works have been conducted to reveal different envelope viruses having their own unique lipid composition (*2*, *7*, *9*, *42*), implying their distinct biological requirements during infection, and suggesting their capacity in sorting specific host lipids into their virus membrane. Two main lipids and a sterol have been described to play a major role for HIV-1 biogenesis and infectivity. PI(4,5)P2 is known to be the plasma membrane lipid targeted by the MA domain of the polyprotein Gag (*5*, *22*, *28*, *43*). SM- and cholesterol-enriched lipid environments, often denoted "raft-like" domains [rafts used to be defined

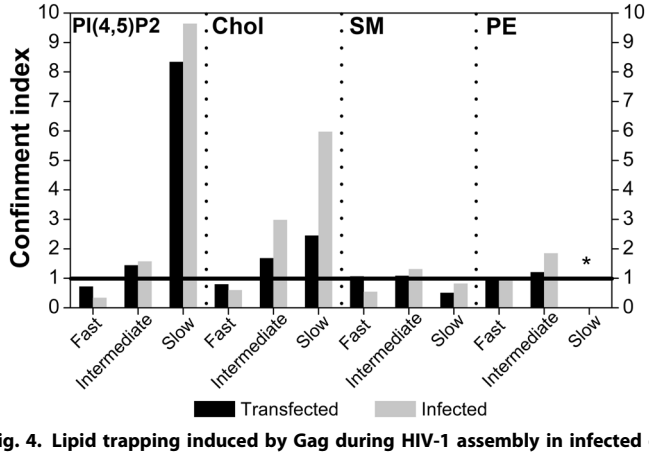

Fig. 4. Lipid trapping induced by Gag during HIV-1 assembly in infected or transfected Jurkat T cells. Confinement indices are based on the relative normalized cumulative frequency distribution of the diffusion coefficients D_a (for D_a = 0.001 to 1 μm²/s, normalized to 100 for D_a = 1 μm²/s), which were arbitrarily divided into three distinct diffusion regimes, slow (D_a < 0.01 μm²/s), intermediate (0.01 ≤ D_a < 0.1 μm²/s), and fast (D_a ≥ 0.1 μm²/s). The sum of cumulative frequencies within each regime resulted in values of the confinement index for each regime as ratio of the latter values for lipid diffusion within and outside the assembly sites or within the assembly sites and noninfected (or nontransfected) cells. Values of the confinement indices found for PI(4,5)P2, Chol, SM, and PE analogs for HIV-1 Gag.eGFP-transfected (black bars) and HIV-1-iGFP–infected (gray bars) Jurkat T cells. Chol and PI(4,5)P2 analogs show strong confinement (indices >1 for intermediate and especially slow regimes) inside assembly sites for both transfected-only or fully infected Jurkat T cells, while neither SM nor PE analogs exhibited confinement inside assembly sites (confinement index ~1 for all regimes). *, no diffusion coefficients below 0.01 μm²/s were observed for PE analogs.

as small (10 to 200 nm), heterogeneous, highly dynamic, sterol- and sphingolipid-enriched domains that compartmentalize cellular processes (*44*)], have also been described as essential for envelope retrieving (*45*), HIV-1 assembly (*24*, *46*, *47*), or infectivity (*26*, *27*).

Whether a preexisting lipid nanodomain or a virus-induced lipid platform is the source of virion lipid membrane during HIV-1 formation is a matter of debate (*36*). We proposed that the Gag protein is the source of the viral lipid envelope upon assembly (*10*, *41*), as also just proposed by another group (*48*). Lipid sorting and lipid domain generation in viral assembly can be identified by nanoscale spatial changes in lipid mobility at the plasma membrane (*13*, *14*), and our super-resolution microscopy–based approaches for the analysis of the lipid dynamics in living cells represent the most relevant model of observation.

In this study, we have determined the diffusion coefficients of fluorescent lipid analogs by applying sSTED-FCS on HIV-1–infected, fluorescent Gag-expressing, and HIV-1–negative $CD4^+$ Jurkat T cells. The sSTED-FCS approach allows for a direct simultaneously quantitative comparison of lipid analog mobility both within and outside assembly sites at the plasma membrane.

In comparison with the plasma membrane of HIV-1–negative cells or plasma membrane regions outside HIV-1 assembly sites, the mobility of PI(4,5)P2 and Chol analogs within viral assembly sites is drastically reduced (up to 10 times decrease of median D_a). The same trend was observed on the assembly site of Gag VLPs in cells expressing only Gag. Although to a less extent than in HIV-1–producing cells, the median values of the diffusion coefficients of PI(4,5)P2 and Chol analogs were significantly reduced in the VLP assembly area. In contrast, the mobility of neither fluorescent SM nor neutral lipid PE analogs exhibited any variation in median values for both HIV-1–producing and Gag VLP–producing cells.

It has been recently shown that diffusion coefficient distributions could unravel the nature of lipid motions (*49*). Therefore, to allow direct comparison of the virus component effect on lipid analog mobility, independently of the cell or the number of expressed component (Gag alone or infectious virus), a confinement index was defined. As in more detail described within the result section, it is based on the relative changes in three different parts of the normalized cumulative distribution of the logarithm of the diffusion coefficients observed inside and outside the virus or VLP assembly site. The value of this confinement index into these three parts reflects the relative change in mobility of the lipid analogs that are trapped (slow, $D_a < 0.01\ \mu m^2/s$), confined (intermediate, $0.01 < D_a < 0.1\ \mu m^2/s$), or freely diffusing (fast, $D_a > 0.1\ \mu m^2/s$) at the assembly sites. By definition, the confinement index will be equal to 1 if no effect occurs on the lipid mobility inside the assembly when compared to outside the assembly site. This unit value was always observed with the fluorescent PE lipid analog, which is generally used as a control of free diffusing lipid in cell plasma membranes (*13*) and is not described as being enriched in HIV-1 envelopes (*1*, *7*).

Among the different fluorescent lipid analogs tested here, the PI(4,5)P2 exhibited the strongest confinement index for the slow part of the distribution, (confinement index, ~10) both for HIV-1 virus and VLP assembly sites in $CD4^+$ T cells. This reveals that the transient binding of PI(4,5)P2 to aggregating Gag conjugated PI(4,5)P2 into the nascent virion or the VLP. This assembly site–specific trapping of PI(4,5)P2 seems to be indeed exclusive to Gag, since the observed confinement indices showed the same trend independent of assembling HIV-1 or VLPs. Moreover, similar confinement indices were observed on the SLB in the in vitro system tested here, i.e., SLBs made of PC, PS, and fluorescent PI(4,5)P2 with or without addition of self-assembling HIV-1 Gag protein (see section S2).

Similar to PI(4,5)P2, the confinement index of the slow diffusing fluorescent Chol analog was also above 1 in infected cells, as well as in transfected cells, confirming that Chol is trapped during HIV-1 assembly and that Gag alone is sufficient to restrict cholesterol mobility at the assembly site. Consequently, the restriction of PI(4,5)P2 and Chol seems to be independent of non-Gag viral proteins, such as HIV-1 Env or accessory/regulatory proteins.

Using in vitro lipid membrane models of different lipid compositions, we recently reported (*10*) that Gag was able to generate TF-PI(4,5)P2 and TF-cholesterol but not TF-SM–enriched lipid nanodomains. This is consistent with data observed here in HIV-1–producing or Gag-expressing $CD4^+$ T cells, even with lipid analogs grafted with different fluorophores. Notably, such local enrichment of PI(4,5)P2 and Chol lipid at virus assembly sites has been predicted using coarse-grained molecular dynamics in the case of the matrix self-assembly of Ebola virus (*50*), implying a potential general mechanism for a number of enveloped viruses that bud from the host cell plasma membrane.

Enrichment of specific lipid in HIV-1 viruses has already been reported (*1*, *2*, *7*), but the mechanism by which these lipids are incorporated into the virus envelope was so far unknown and has now been discussed by our present work and the one just released by Sengupta *et al.* (*48*). Different values of virion lipid enrichment have been found, depending on the cell lines and the biochemical methods to purify viruses or isolate plasma membranes from the other cell membranes (*1*, *2*, *7*). In H9 T lymphocytes, Chan *et al.* (*2*) have shown that HIV-1 lipid envelope is two times higher in PI(4,5)P2 and three times higher in cholesterol when compared to the plasma membrane of the HIV-1–producing H9 cells. Our results show that this enrichment occurs during virus assembly. Sequestration of PI(4,5)P2 in the plasma membrane in the vicinity of PI(4,5)P2 binding proteins or peptide has already been shown and modeled a decade ago (*51*). Using coarse-grained dynamic modeling, we also previously reported the sequestration of PI(4,5)P2 upon binding of the MA domain of Gag to lipid membranes. Given that PI(4,5)P2 is important for the binding of Gag to the cell plasma membrane (*5*), the clustering of PI(4,5)P2 at the cell membrane may provide an additional mechanism to further concentrate Gag, thereby enhancing virus assembly. Furthermore, molecular simulations of PI(4,5)P2 clustering have revealed the induction of negative membrane curvature (*52*) by PI(4,5)P2, which could facilitate the formation of spherical particle morphogenesis during virus assembly.

Cholesterol has been shown to play a role in HIV-1 Gag matrix domain (MA) binding to membranes (*8*, *53*), as well as in the stabilization of PI(4,5)P2 lipid nanodomains in the absence of proteins (*52*). A role for the Chol can be proposed on the basis of the work of Doktorova *et al.* (*54*) on Rous sarcoma virus MA-membrane interactions, which can be generalized to other retroviruses. Using molecular dynamics simulations, Doktorova and collaborators showed that the MA domain of the retroviral Gag protein interacts better with the charged head of phosphatidylserine (PS) phospholipids of the membrane in the presence of Chol. They proposed that Chol would increase lipid packing and membrane surface charge density, facilitating MA association to membrane. We previously reported the concomitant trapping of Chol and PI(4,5)P2 analogs by HIV-1 Gag in vitro on SLBs upon Gag multimerization (*10*). Thus, the trapping of both PI(4,5)P2 and Chol by

HIV-1 Gag that we observe in CD4 T cells could also favor Chol enhancing locally PI(4,5)P2 clustering and making membrane surface more negative: This combination would favor the targeting and the next assembling of Gag molecules at the viral bud through the enhancing of MA positively charged membrane interactions.

It has been suggested for a long time that preexisting SM-Chol–enriched cell plasma membrane domains (so-called "raft" domains) could play a role in HIV-1 assembly [reviewed in (*45*)]. The recently released work of Sengupta *et al.* (*48*) proposed that, during Gag self-assembly in adherent cells, the immobilization of PI(4,5)P2, naturally bearing a long C18 acyl chain in the *sn-1* position, could generate transbilayer coupling by means of an interdigitation mechanism with the SM acyl chains, inducing the recruitment of the SM-Chol enriched domains present in the outer leaflet and leading, therefore, to specific recruitment in the budding site of raft-partitioning proteins. To verify this hypothesis in T cells, we also assessed changes in fluorescent SM analog dynamics at the virus assembly site using our sSTED-FCS approach. The observed confinement indices of the SM analog were never above 1, highlighting that HIV-1 assembly had no direct effect on the SM mobility at the $CD4^+$ T cell plasma membrane. Our results, considering this lack of SM enrichment in CD4 T cells at the HIV-1 budding sites, is in line with recent lipidomics data (*7*), our previous finding of SM exclusion during the time course of HIV-1 Gag assembly on SLBs (*10*), and the already observed exclusion of SM in curved membranes (*55*). The exact role of SM in HIV-1 assembly in T cells is therefore still an open question (*56*).

Cholesterol has also been proposed to play a major role in interleaflet coupling of lipid membranes (*57*). Thallmair *et al.* (*58*) has shown that cholesterol could serve as an efficient signaling molecule transferring information between the leaflets while populating the interleaflet space. It has been previously shown that cholesterol was enriched at the center of polyunsaturated lipid membranes, an acyl chain naturally present in the *sn-2* position of PI(4,5)P2 (*59*). This possible repositioning of cholesterol in the middle of the membrane, due to the strong PI(4,5)P2 trapping at the budding site, will facilitate cholesterol flip-flop, resulting in its local enrichment in the outer leaflet and the generation of an outer leaflet liquid-ordered domain without the need of any additional SM.

Overall, our results provide direct evidence that HIV-1 Gag assembly drives the lipid sorting in host CD4 T cell plasma membranes and creates its own PI(4,5)P2/cholesterol lipid-enriched membrane environment likely to provide a positive feedback loop to recruit additional Gag proteins at the budding site through the PI(4,5)P2-MA domain of Gag interactions for the biogenesis of HIV-1 particles. Moreover, the cholesterol enrichment observed here could play a major role in the lipid bilayer transmembrane coupling mechanism needed to retrieve specific HIV-1 envelope proteins.

MATERIALS AND METHODS

Experimental design

The main goal of this study was to unravel whether the viral Gag protein is targeted toward preexisting lipid domains at the host cell plasma membrane that will help in HIV-1 assembly,or whether, in the opposite, Gag creates its own lipid domain during virus formation. To do so, we measured the change in mobility of different lipid analogs at HIV-1 assembly sites. We used fluorescent lipid analogs described to play a role either in Gag membrane targeting [PI(4,5)P2] and assembly (cholesterol) or known to be a part of preexisting lipid domains at the plasma membrane (SM) and, finally, a control lipid (PE) not described to play a role in any of the two possible mechanisms. To achieve our goal, our experimental setup was based on a direct measurement of apparent diffusion coefficient of the lipid analogs inside and outside HIV-1 fluorescent Gag assembly sites using spatial scanning FCS on a super-resolution STED microscope (delivering an observation spot size of around 100 nm in diameter, i.e., below that of a conventional microscope). Our measurements were performed in HIV-1–infected CD4 T cells and as a control in CD4 T cells expressing Gag-iGFP only. Last, using a top-bottom approach of purified HIV-1 Gag on fluorescent PI(4,5)P2-SLBs, we could highlight that Gag was sufficient to generate a PI(4,5)P2-nanodomain platform for assembly.

Lipids and fluorescent lipid analogs

Lipids 1,2-dioleoyl-*sn*-glycero-3-phosphocholine (DOPC), brain L-α-PS, and brain PI(4,5)P2 were purchased from Avanti Polar Lipids (Alabaster, AL, USA). ATTO647N-DPPE and ATTO647N–SM (ATTO647N-SM) were purchased from ATTO-TEC GmbH (Siegen-Weidenau, Siegen, Germany). Abberior STAR RED (KK114)–1,2-dihexadecanoyl-*sn*-glycero-3-phosphoethanolamine (KK114-DPPE), cholesterol–PEG(1 k)-Abberior STAR RED (KK114) [Chol-PEG(1 k)-KK114], and ATTO647N-PI(4,5)P2 [ATTO647N-PI(4,5)P2] were all purchased from Abberior GmbH (Göttingen, Germany). Chemical structures of all the lipid analogs used in this study are given in fig. S1.

Gag protein and SLBs

Full-length Gag protein had been produced and purified as described previously (*10*). SLBs for Gag lipid clustering measurements were prepared from 30-nm small unilamellar vesicles (SUVs) with the following: DOPC, 68%; PS, 30%; PI(4,5)P2, 1.9%; and ATTO647N-PI(4,5)P2, 0.1% mol at 0.1 mg/ml in a citrate buffer [10 mM Na citrate, 100 mM NaCl, and 0.5 mM EGTA (pH 4.6)]. The SUVs were then spread for 45 min at 37°C on coverslips pretreated by sonication in 5% SDS solution and incubation for 30 min in freshly made piranha solution (H2SO4:H202 2:1 vol). After disposition of the SLBs, scanning FCS measurements were performed and again 15 min after Gag was added at 1 μM final concentration.

Plasmids

Plasmid expressing fully infectious Jurkat T cell tropic NL4.3 HIV-1 Gag-iGFP was previously described (*31*) and was a gift from B. Chen. Plasmid expressing NL4.3 HIV-1 Gag-eGFP fusion protein was previously described (*60*) and was a gift from H. de Rocquigny.

Cell culture

Jurkat T cells (human T cell leukemia cell line–ATCC TIB-152) were grown in RPMI 1640 with GlutaMAX (Gibco), supplemented with 10% fetal calf serum, and penicillin-streptomycin (100 U/ml) and 20 mM Hepes (pH 7.4). Cells were maintained at 37°C, 5% CO_2.

NL4.3 HIV-1 Gag.iGFP particle preparation

Fully infectious NL4.3 HIV-1 Gag-iGFP particles were prepared from the tissue culture supernatant of 293 T cells transfected using polyethyleneimine with 15 μg of pNL4.3 HIV-1 Gag-iGFP plasmid. Tissue culture supernatants were harvested 48 hours after transfection, and particles were concentrated using a Lenti-X Concentrator reagent (Clontech) according to the manufacturer's instructions. Concentrated particles were snap-frozen and stored in aliquots at −80°C.

Jurkat T cell infection

Jurkat CD4$^+$ T cells were infected by incubation of 1 million cells with HIV-1 NL4.3 Gag-iGFP particles in 50 µl of RPMI medium for 1 hour at 37°C. Cells were washed three times in RPMI medium and then cultured for 72 hours at 2 million cells per milliliter to achieve a 5 to 10% infection rate with progeny virus production.

Jurkat T cell transfection

Jurkat T cells (2×10^6) were microporated with 4 µg of plasmid expressing NL4.3 HIV-1 Gag.eGFP using the AMAXA system (Lonza), as previously described in (*33*). After microporation, Jurkat T cells were incubated in RPMI complete medium and harvested 24 hours after transfection for microscopy acquisitions as described in the following sections. For supplemental information concerning the choice of the transfected Jurkat T cells expressing Gag.eGFP, see fig. S6.

Microscope setup

sSTED-FCS measurements were performed on the Abberior Instrument Expert Line STED super-resolution microscope (Abberior Instruments GmbH, Göttingen, Germany) using 485- and 640-nm pulsed excitation laser sources and a pulsed STED laser operating at 775 nm and an 80-MHz repetition rate. The fluorescence excitation and collection were performed using a 100×/1.40 numerical aperture (NA) UPlanSApo oil immersion objective (Olympus Industrial, Southend-on-Sea, UK). All acquisition operations were controlled by Imspector software (Abberior Instruments GmbH), and point FCS data for the calibration of the observation spot sizes were recorded using a hardware correlator (Flex02-08D, correlator.com, operated by the company's software).

Confocal microscope FCS measurements were performed on a Zeiss LSM 780 (Zeiss, Iena, Germany) using a HeNe 633-nm laser as the excitation source. Fluorescence excitation and collection were performed using a 63×/1.40-NA PlanApo oil immersion objective (Zeiss). Acquisition operations were controlled by the Zeiss Zen software. Point FCS was used to calibrate the observation spot with the LSM 780 internal hardware correlator.

Microscope sample preparation

For calibration of the observation spot sizes using STED-FCS, SLBs were prepared, as previously described (*61*), by spin-coating a coverslip with a solution of DOPC (1 mg/ml) and KK114-DPPE (0.5 µg/ml) in $CHCl_3$/MeOH. Coverslips were cleaned by piranha solution (3:1 sulfuric acid and hydrogen peroxide). The lipid bilayer was formed by rehydrating with SLB buffer containing 10 mM Hepes and 150 mM NaCl (pH 7.4). Calibration of the confocal observation spot size was made with a 50 nM solution of rhodamine in pure water using D = 280 µm^2/s as the diffusion coefficient.

For lipid mobility measurements inside and outside Gag assembly sites in mammalian cells, 3×10^5 Jurkat T cells 72 hours after infection with NL4.3 HIV-1 Gag-iGFP virus particles or 24 hours after transfection with NL4.3 HIV-1 Gag-eGFP–expressing plasmid were resuspended in 200 µl of Leibovitz's L-15 medium (Sigma-Aldrich) and incubated with 25 nM of the indicated fluorescent lipid analog probe for 5 min at 37°C. Cells were then washed three times in suspension in L-15 medium, resuspended in 250 µl of L-15 medium, and adhered to solution poly-L-lysine (0.1 mg/ml) (Sigma-Aldrich)–coated glass surface of eight-well Ibidi µ-Slides (Ibidi, Martinsried, Germany) at 37°C 30 min prior to microscopy measurements.

For lipid mobility measurements on myr(−) Gag containing SLBs, prior to experiments, citrate buffer was changed to protein buffer [10 mM Hepes (pH 7.4), 150 mM KCl, and 2 mM EDTA], followed by injection of 1 µM myr(−) Gag.

sSTED-FCS signal acquisition

sSTED-FCS data of the lipid mobility inside and outside Gag assembly sites in Jurkat T cells were acquired at 37°C using fluorescent Gag signal as a guide. Fluorescent lipid signal intensity fluctuation carpets (scanning an orbit multiple times) were recorded using the Imspector software with the following parameters: orbital scan frequency, 3.23 kHz; scan orbit length, 1.5 µm; pixel dwell time, 10 µs; total measurement time, 10 s; pixel size, 50 nm per pixel, 10-µW excitation power (back aperture), 640 nm; and observation spot diameter, 100 nm (full width at half maximum) FWHM (as determined by SLB calibration measurements; section S1). The scan frequency selected for these experiments was set sufficiently high to enable the extraction of the diffusion dynamics of fluorescent lipid analogs in the cell plasma membrane (*14*).

FCS curve autocorrelation and fitting

The FoCuS-scan software (*40*) was used to autocorrelate the sSTED-FCS data and to fit it with a classical 2D diffusion model

$$G_N(\tau) = G(\infty) + G_N(0)\left[1 + \frac{\tau}{t_{xy}}\right]^{-1} \quad (1)$$

where $G_N(\tau)$ is the correlation function at time lag τ, $G(\infty)$ is the offset, $G_N(0)$ is the amplitude, and t_{xy} is the average lateral transit time through the observation spot. As done in all previous sSTED-FCS measurements, we left out anomaly factors in the fitting equation (as often done in nonscanning single-point STED-FCS data), since the decay of the sSTED-FCS curves starts at 0.5- to 1-ms correlation times only and because anomaly is much better revealed by comparing (cumulative) frequency histograms of resulting parameters (*14*). Last, regarding the noise in our correlogram, we discarded all the fitted correlations times smaller than 2 ms, resulting in a truncated distibution of the correlation times. The corresponding values of the apparent molecular diffusion coefficient (D_a) were calculated from t_{xy}

$$D_a = \mathrm{FWHM}^2/8\ln(2)t_{xy} \quad (2)$$

where FWHM represents the usual full-width half maximum of the observation spot (100 nm; see section S4).

Calculation of the confinement index

Diffusion coefficients obtained for the different lipid in the different conditions tested were binned in groups every 10^{-3} µm^2/s from 0 to 1.2 µm^2/s. The distribution was cumulated and normalized. It was then split into three parts: slow ($D_a < 10^{-2}$ µm^2/s), intermediate ($10^{-2} \leq D_a < 10^{-1}$ µm^2/s), and fast ($D_a \geq 10^{-1}$ µm^2/s). The relative proportion (Pi) of the total distribution ($0 \leq \mathrm{Pi} \leq 1$) of each of these parts was then calculated for each molecule inside the assembly site, outside the assembly site, and in noninfected or transfected cells. The confinement index is defined for each of the three parts as the quotient of the Pi value found inside the assembly site over

the Pi value found outside the assembly site or in noninfected or transfected cells (Fig. 4).

Statistical analysis

Because of the non-Gaussian nature of the diffusion coefficient data distribution, Wilcoxon rank sum test was used with the result $P < 0.05$ considered statistically significant. Statistical tests were performed using GraphPad Prism software. Power calculations confirmed that, for chosen sample sizes, the power of a two-sided hypothesis test at the 0.05 significance was over 90%. In all compared groups, IQR serves as an estimate of variation. IQRs were similar in all compared groups.

SUPPLEMENTARY MATERIALS

Supplementary material for this article is available at http://advances.sciencemag.org/cgi/content/full/5/10/eaaw8651/DC1

Sections S1 and S2. Characterization of fluorescent lipid analogs

Section S3. MHC-I mobility at HIV-1 assembly sites in NL4.3 Gag-iGFP HIV-1–infected Jurkat T cells

Section S4. STED microscope calibration

Section S5. PI(4,5)P2 clustering and trapping by full-length HIV-1 Gag on biomimetic membranes

Section S6. Budding efficiency comparison in Jurkat T cells transfected with Gag.eGFP or with a mixture of Gag.eGFP/Gag (ratio, 1:3)

Section S7. Cumulative frequency distributions observed in infected cells for the different lipids

Section S8. Cumulative frequency distributions observed in transfected cells for the different lipids

Fig. S1. Fluorescent lipid analog structures.

Fig. S2. Fluorescent lipid analog mobility in Jurkat T cells.

Fig. S3. MHC-I mobility at HIV-1 assembly sites in NL4.3 Gag-iGFP HIV-1–infected Jurkat T cells.

Fig. S4. STED microscope calibration results.

Fig. S5. Changes in the lateral mobility of ATTO647N-PI(4,5)P2 upon addition of Gag on SLBs.

Fig. S6. Jurkat T cell coelectroporation with Gag.eGFP and Gag plasmids.

Fig. S7. Cumulative frequency distributions of diffusion coefficient observed in HIV-1–infected T cells.

Fig. S8. Cumulative frequency distributions of diffusion coefficient observed in HIV-1 Gag-transfected T cells.

Movie S1. Drift stabilized time lapse movie of a representative NL4.3 Gag-iGFP HIV-1–infected Jurkat T-cell showing already present and newly developing virus assembly sites.

References (*62*, *63*)

REFERENCES AND NOTES

1. B. Brügger, B. Glass, P. Haberkant, I. Leibrecht, F. T. Wieland, H. G. Kräusslich, The HIV lipidome: A raft with an unusual composition. *Proc. Natl. Acad. Sci. U.S.A.* **103**, 2641–2646 (2006).
2. R. Chan, P. D. Uchil, J. Jin, G. Shui, D. E. Ott, W. Mothes, M. R. Wenk, Retroviruses human immunodeficiency virus and murine leukemia virus are enriched in phosphoinositides. *J. Virol.* **82**, 11228–11238 (2008).
3. J. Chojnacki, D. Waithe, P. Carravilla, N. Huarte, S. Galiani, J. Enderlein, C. Eggeling, Envelope glycoprotein mobility on HIV-1 particles depends on the virus maturation state. *Nat. Commun.* **8**, 545 (2017).
4. W. Zhou, L. J. Parent, J. W. Wills, M. D. Resh, Identification of a membrane-binding domain within the amino-terminal region of human immunodeficiency virus type 1 Gag protein which interacts with acidic phospholipids. *J. Virol.* **68**, 2556–2569 (1994).
5. A. Ono, S. D. Ablan, S. J. Lockett, K. Nagashima, E. O. Freed, Phosphatidylinositol (4,5) bisphosphate regulates HIV-1 Gag targeting to the plasma membrane. *Proc. Natl. Acad. Sci. U.S.A.* **101**, 14889–14894 (2004).
6. A. Ono, D. Demirov, E. O. Freed, Relationship between human immunodeficiency virus type 1 Gag multimerization and membrane binding. *J. Virol.* **74**, 5142–5150 (2000).
7. M. Lorizate, T. Sachsenheimer, B. Glass, A. Habermann, M. J. Gerl, H.-G. Kräusslich, B. Brügger, Comparative lipidomics analysis of HIV-1 particles and their producer cell membrane in different cell lines. *Cell. Microbiol.* **15**, 292–304 (2013).
8. R. A. Dick, S. L. Goh, G. W. Feigenson, V. M. Vogt, HIV-1 Gag protein can sense the cholesterol and acyl chain environment in model membranes. *Proc. Natl. Acad. Sci. U.S.A.* **109**, 18761–18766 (2012).
9. H. Keller, H.-G. Kräusslich, P. Schwille, Multimerizable HIV Gag derivative binds to the liquid-disordered phase in model membranes. *Cell. Microbiol.* **15**, 237–247 (2013).
10. N. Yandrapalli, Q. Lubart, H. S. Tanwar, C. Picart, J. Mak, D. Muriaux, C. Favard, Self assembly of HIV-1 Gag protein on lipid membranes generates $PI(4,5)P_2$/Cholesterol nanoclusters. *Sci. Rep.* **6**, 39332 (2016).
11. B. Olety, S. L. Veatch, A. Ono, Phosphatidylinositol-(4,5)-bisphosphate acyl chains differentiate membrane binding of HIV-1 Gag from that of the phospholipase Cδ1 pleckstrin homology domain. *J. Virol.* **89**, 7861–7873 (2015).
12. E. Barklis, A. O. Staubus, A. Mack, L. Harper, R. L. Barklis, A. Alfadhli, Lipid biosensor interactions with wild type and matrix deletion HIV-1 Gag proteins. *Virology* **518**, 264–271 (2018).
13. C. Eggeling, C. Ringemann, R. Medda, G. Schwarzmann, K. Sandhoff, S. Polyakova, V. N. Belov, B. Hein, C. von Middendorff, A. Schönle, S. W. Hell, Direct observation of the nanoscale dynamics of membrane lipids in a living cell. *Nature* **457**, 1159–1162 (2009).
14. A. Honigmann, V. Mueller, H. Ta, A. Schoenle, E. Sezgin, S. W. Hell, C. Eggeling, Scanning STED-FCS reveals spatiotemporal heterogeneity of lipid interaction in the plasma membrane of living cells. *Nat. Commun.* **5**, 5412 (2014).
15. A. Benda, Y. Ma, K. Gaus, Self-calibrated line-scan STED-FCS to quantify lipid dynamics in model and cell membranes. *Biophys. J.* **108**, 596–609 (2015).
16. I. Urbančič, J. Brun, D. Shrestha, D. Waithe, C. Eggeling, J. Chojnacki, Lipid composition but not curvature is the determinant factor for the low molecular mobility observed on the membrane of virus-like vesicles. *Viruses* **10**, E415 (2018).
17. B. Olety, A. Ono, Roles played by acidic lipids in HIV-1 Gag membrane binding. *Virus Res.* **193**, 108–115 (2014).
18. D. Muriaux, J.-L. Darlix, Properties and functions of the nucleocapsid protein in virus assembly. *RNA Biol.* **7**, 744–753 (2010).
19. E. O. Freed, HIV-1 assembly, release and maturation. *Nat. Rev. Microbiol.* **13**, 484–496 (2015).
20. S. A. K. Datta, X. Zuo, P. K. Clark, S. J. Campbell, Y.-X. Wang, A. Rein, Solution properties of murine leukemia virus Gag protein: Differences from HIV-1 Gag. *J. Virol.* **85**, 12733–12741 (2011).
21. N. Kempf, V. Postupalenko, S. Bora, P. Didier, Y. Arntz, H. de Rocquigny, Y. Mély, The HIV-1 nucleocapsid protein recruits negatively charged lipids to ensure its optimal binding to lipid membranes. *J. Virol.* **89**, 1756–1767 (2015).
22. V. Chukkapalli, I. B. Hogue, V. Boyko, W.-S. Hu, A. Ono, Interaction between the human immunodeficiency virus type 1 Gag matrix domain and phosphatidylinositol-(4,5)-bisphosphate is essential for efficient gag membrane binding. *J. Virol.* **82**, 2405–2417 (2008).
23. F. Mücksch, V. Laketa, B. Müller, C. Schultz, H.-G. Kräusslich, Synchronized HIV assembly by tunable PIP_2 changes reveals PIP_2 requirement for stable Gag anchoring. *eLife* **6**, e25287 (2017).
24. A. Ono, E. O. Freed, Plasma membrane rafts play a critical role in HIV-1 assembly and release. *Proc. Natl. Acad. Sci. U.S.A.* **98**, 13925–13930 (2001).
25. D. H. Nguyen, J. E. K. Hildreth, Evidence for budding of human immunodeficiency virus type 1 selectively from glycolipid-enriched membrane lipid rafts. *J. Virol.* **74**, 3264–3272 (2000).
26. D. Hawkes, K. L. Jones, R. P. Smyth, C. F. Pereira, R. Bittman, A. Jaworowski, J. Mak, Properties of HIV-1 associated cholesterol in addition to raft formation are important for virus infection. *Virus Res.* **210**, 18–21 (2015).
27. S. Campbell, K. Gaus, R. Bittman, W. Jessup, S. Crowe, J. Mak, The raft-promoting property of virion-associated cholesterol, but not the presence of virion-associated Brij 98 rafts, is a determinant of human immunodeficiency virus type 1 infectivity. *J. Virol.* **78**, 10556–10565 (2004).
28. J. S. Saad, J. Miller, J. Tai, A. Kim, R. H. Ghanam, M. F. Summers, Structural basis for targeting HIV-1 Gag proteins to the plasma membrane for virus assembly. *Proc. Natl. Acad. Sci. U.S.A.* **103**, 11364–11369 (2006).
29. L. Charlier, M. Louet, L. Chaloin, P. Fuchs, J. Martinez, D. Muriaux, C. Favard, N. Floquet, Coarse-grained simulations of the HIV-1 matrix protein anchoring: Revisiting its assembly on membrane domains. *Biophys. J.* **106**, 577–585 (2014).
30. P. Y. Mercredi, N. Bucca, B. Loeliger, C. R. Gaines, M. Mehta, P. Bhargava, P. R. Tedbury, L. Charlier, N. Floquet, D. Muriaux, C. Favard, C. R. Sanders, E. O. Freed, J. Marchant, M. F. Summers, Structural and molecular determinants of membrane binding by the HIV-1 matrix protein. *J. Mol. Biol.* **428**, 1637–1655 (2016).
31. W. Hubner, P. Chen, A. D. Portillo, Y. Liu, R. E. Gordon, B. K. Chen, Sequence of human immunodeficiency virus type 1 (HIV-1) Gag localization and oligomerization monitored with live confocal imaging of a replication-competent, fluorescently tagged HIV-1. *J. Virol.* **81**, 12596–12607 (2007).
32. S. Ivanchenko, W. J. Godinez, M. Lampe, H. G. Kräusslich, R. Eils, K. Rohr, C. Bräuchle, B. Müller, D. C. Lamb, Dynamics of HIV-1 assembly and release. *PLOS Pathog.* **5**, e1000652 (2009).

33. C. Floderer, J.-B. Masson, E. Boilley, S. Georgeault, P. Merida, M. el Beheiry, M. Dahan, P. Roingeard, J.-B. Sibarita, C. Favard, D. Muriaux, Single molecule localisation microscopy reveals how HIV-1 Gag proteins sense membrane virus assembly sites in living host CD4 T cells. *Sci. Rep.* **8**, 16283 (2018).
34. V. Mueller, C. Ringemann, A. Honigmann, G. Schwarzmann, R. Medda, M. Leutenegger, S. Polyakova, V. N. Belov, S. W. Hell, C. Eggeling, STED nanoscopy reveals molecular details of cholesterol- and cytoskeleton-modulated lipid interactions in living cells. *Biophys. J.* **101**, 1651–1660 (2011).
35. V. Mueller, A. Honigmann, C. Ringemann, R. Medda, G. Schwarzmann, C. Eggeling, FCS in STED microscopy: Studying the nanoscale of lipid membrane dynamics. *Methods Enzymol.* **519**, 1–38 (2013).
36. E. Mobarak, M. Javanainen, W. Kulig, A. Honigmann, E. Sezgin, N. Aho, C. Eggeling, T. Rog, I. Vattulainen, How to minimize dye-induced perturbations while studying biomembrane structure and dynamics: PEG linkers as a rational alternative. *Biochim. Biophys. Acta Biomembr.* **1860**, 2436–2445 (2018).
37. E. Sezgin, F. B. Can, F. Schneider, M. P. Clausen, S. Galiani, T. A. Stanly, D. Waithe, A. Colaco, A. Honigmann, D. Wüstner, F. Platt, C. Eggeling, A comparative study on fluorescent cholesterol analogs as versatile cellular reporters. *J. Lipid Res.* **57**, 299–309 (2016).
38. E. Sezgin, I. Levental, M. Grzybek, G. Schwarzmann, V. Mueller, A. Honigmann, V. N. Belov, C. Eggeling, Ü. Coskun, K. Simons, P. Schwille, Partitioning, diffusion, and ligand binding of raft lipid analogs in model and cellular plasma membranes. *Biochim. Biophys. Acta* **1818**, 1777–1784 (2012).
39. J. Schneider, J. Zahn, M. Maglione, S. J. Sigrist, J. Marquard, J. Chojnacki, H.-G. Kräusslich, S. J. Sahl, J. Engelhardt, S. W. Hell, Ultrafast, temporally stochastic STED nanoscopy of millisecond dynamics. *Nat. Methods* **12**, 827–830 (2015).
40. D. Waithe, F. Schneider, J. Chojnacki, M. P. Clausen, D. Shrestha, J. B. de la Serna, C. Eggeling, Optimized processing and analysis of conventional confocal microscopy generated scanning FCS data. *Methods* **140–141**, 62–73 (2018).
41. A. Kerviel, A. Thomas, L. Chaloin, C. Favard, D. Muriaux, Virus assembly and plasma membrane domains: Which came first? *Virus Res.* **171**, 332–340 (2013).
42. M. J. Gerl, J. L. Sampaio, S. Urban, L. Kalvodova, J. M. Verbavatz, B. Binnington, D. Lindemann, C. A. Lingwood, A. Shevchenko, C. Schroeder, K. Simons, Quantitative analysis of the lipidomes of the influenza virus envelope and MDCK cell apical membrane. *J. Cell Biol.* **196**, 213–221 (2012).
43. V. Chukkapalli, A. Ono, Molecular determinants that regulate plasma membrane association of HIV-1 Gag. *J. Mol. Biol.* **410**, 512–524 (2011).
44. L. J. Pike, Rafts defined: A report on the Keystone symposium on lipid rafts and cell function. *J. Lipid Res.* **47**, 1597–1598 (2006).
45. K. Leung, J. O. Kim, L. Ganesh, J. Kabat, O. Schwartz, G. J. Nabel, HIV-1 assembly: Viral glycoproteins segregate quantally to lipid rafts that associate individually with HIV-1 capsids and virions. *Cell Host Microbe* **3**, 285–292 (2008).
46. A. A. Waheed, E. O. Freed, Lipids and membrane microdomains in HIV-1 replication. *Virus Res.* **143**, 162–176 (2009).
47. W. I. Sundquist, H.-G. Kräusslich, HIV-1 assembly, budding, and maturation. *Cold Spring Harb. Perspect. Med.* **2**, a006924 (2012).
48. P. Sengupta, A. Y. Seo, H. A. Pasolli, Y. E. Song, M. C. Johnson, J. Lippincott-Schwartz, A lipid-based partitioning mechanism for selective incorporation of proteins into membranes of HIV particles. *Nat. Cell Biol.* **21**, 452–461 (2019).
49. F. Schneider, D. Waithe, B. C. Lagerholm, D. Shrestha, E. Sezgin, C. Eggeling, M. Fritzsche, Statistical analysis of scanning fluorescence correlation spectroscopy data differentiates free from hindered diffusion. *ACS Nano* **12**, 8540–8546 (2018).
50. J. B. Gc, B. S. Gerstman, R. V. Stahelin, P. P. Chapagain, The Ebola virus protein VP40 hexamer enhances the clustering of PI(4,5)P_2 lipids in the plasma membrane. *Phys. Chem. Chem. Phys.* **18**, 28409–28417 (2016).
51. J. Wang, A. Gambhir, S. McLaughlin, D. Murray, A computational model for the electrostatic sequestration of PI(4,5)P_2 by membrane-adsorbed basic peptides. *Biophys. J.* **86**, 1969–1986 (2004).
52. H. Koldsø, D. Shorthouse, J. Hélie, M. S. P. Sansom, Lipid clustering correlates with membrane curvature as revealed by molecular simulations of complex lipid bilayers. *PLOS Comput. Biol.* **10**, e1003911 (2014).
53. M. Barros, F. Heinrich, S. A. K. Datta, A. Rein, I. Karageorgos, H. Nanda, M. Lösche, Membrane binding of HIV-1 matrix protein: Dependence on bilayer composition and protein lipidation. *J. Virol.* **90**, 4544–4555 (2016).
54. M. Doktorova, F. A. Heberle, R. L. Kingston, G. Khelashvili, M. A. Cuendet, Y. Wen, J. Katsaras, G. W. Feigenson, V. M. Vogt, R. A. Dick, Cholesterol promotes protein binding by affecting membrane electrostatics and solvation properties. *Biophys. J.* **113**, 2004–2015 (2017).
55. B. Sorre, A. Callan-Jones, J. B. Manneville, P. Nassoy, J. F. Joanny, J. Prost, B. Goud, P. Bassereau, Curvature-driven lipid sorting needs proximity to a demixing point and is aided by proteins. *Proc. Natl. Acad. Sci. U.S.A.* **106**, 5622–5626 (2009).
56. J. Podkalicka, P. Bassereau, How membrane physics rules the HIV envelope. *Nat. Cell Biol.* **21**, 413–415 (2019).
57. M. D. Collins, Interleaflet coupling mechanisms in bilayers of lipids and cholesterol. *Biophys. J.* **94**, L32–L34 (2008).
58. S. Thallmair, H. I. Ingólfsson, S. J. Marrink, Cholesterol flip-flop impacts domain registration in plasma membrane models. *J. Phys. Chem. Lett.* **9**, 5527–5533 (2018).
59. T. A. Harroun, J. Katsaras, S. R. Wassall, Cholesterol hydroxyl group is found to reside in the center of a polyunsaturated lipid membrane. *Biochemistry* **45**, 1227–1233 (2006).
60. S. E. El Meshri, D. Dujardin, J. Godet, L. Richert, C. Boudier, J. L. Darlix, P. Didier, Y. Mély, H. de Rocquigny, Role of the nucleocapsid domain in HIV-1 Gag oligomerization and trafficking to the plasma membrane: A fluorescence lifetime imaging microscopy investigation. *J. Mol. Biol.* **427**, 1480–1494 (2015).
61. M. P. Clausen, E. Sezgin, J. Bernardino de la Serna, D. Waithe, B. C. Lagerholm, C. Eggeling, A straightforward approach for gated STED-FCS to investigate lipid membrane dynamics. *Methods* **88**, 67–75 (2015).
62. N. Jouvenet, P. D. Bieniasz, S. M. Simon, Imaging the biogenesis of individual HIV-1 virions in live cells. *Nature* **454**, 236–240 (2008).
63. B. Müller, J. Daecke, O. T. Fackler, M. T. Dittmar, H. Zentgraf, H.-G. Krausslich, Construction and characterization of a fluorescently labeled infectious human immunodeficiency virus type 1 derivative. *J. Virol.* **78**, 10803–10813 (2004).

Acknowledgments: We would like to thank T. J. Hope (Northwestern University, Chicago) and the Department of NanoBiophotonics (Max Planck Institute for Biophysical Chemistry, Gottingen, Germany) for the eGFP.Vpr construct. We would also like to thank the Montpellier RIO Imaging facilities (MRI, Montpellier France), especially M.-P. Blanchard from IGF (CNRS Montpellier) and the Wolfson Imaging Centre Oxford (UK), for help with the use of microscopes. C.F. and D.M. are members of the CNRS consortium ImaBIO, France. **Funding:** The overall project was funded by CNRS and the French National Agency for Research (ANR "FLUOBUDS," ANR-13-BSV5-0006-01, and ANR Q-PiD-AAP2017) and the French Agency against AIDS (ANRS) (grant number ECTZ37578). J.C. and C.E. were supported by the Medical Research Council (grant number MC_UU_12010/unit programs G0902418 and MC_UU_12025), MRC/BBSRC/EPSRC (grant number MR/K01577X/1), Wellcome Trust (grant number 104924/14/Z/14), Deutsche Forschungsgemeinschaft (Research unit 1905 "Structure and function of the peroxisomal translocon", Jena Excellence Cluster "Balance of the Microverse", Collaborative Research Center 1278), and Oxford internal funds (EPA Cephalosporin Fund and John Fell Fund). J.M. is a recipient of funding from Australian National Health and Medical Research Council project grants App543107 and App1121697 and is a subawardee of National Institutes of Health NIH RO1 GM064347. **Author contributions:** C.F., J.C., C.E., and D.M. designed the study. D.M., C.F., J.C., P.M., and N.Y. performed the experiments. J.M. provided the recombinant myr(−) Gag protein. C.F. developed the confinement index analysis. C.F., J.C., and C.E. analyzed the STED-FCS data. J.C., C.F., D.M., and C.E. wrote the manuscript. All authors contributed in discussing the data, experiments, and the manuscript. **Competing interests:** The authors declare that they have no competing interests. **Data and materials availability:** All data needed to evaluate the conclusions in the paper are present in the paper and/or the Supplementary Materials. Additional data related to this paper may be requested from the authors.

Submitted 31 January 2019
Accepted 9 September 2019
Published 2 October 2019
10.1126/sciadv.aaw8651

Citation: C. Favard, J. Chojnacki, P. Merida, N. Yandrapalli, J. Mak, C. Eggeling, D. Muriaux, HIV-1 Gag specifically restricts PI(4,5)P2 and cholesterol mobility in living cells creating a nanodomain platform for virus assembly. *Sci. Adv.* **5**, eaaw8651 (2019).

Science Advances

HIV-1 Gag specifically restricts PI(4,5)P2 and cholesterol mobility in living cells creating a nanodomain platform for virus assembly

C. Favard, J. Chojnacki, P. Merida, N. Yandrapalli, J. Mak, C. Eggeling and D. Muriaux

Sci Adv **5** (10), eaaw8651.
DOI: 10.1126/sciadv.aaw8651

Science Advances (ISSN 2375-2548) is published by the American Association for the Advancement of Science, 1200 New York Avenue NW, Washington, DC 20005. The title *Science Advances* is a registered trademark of AAAS.